# Anomalous lattice response at the Mott Transition in a Quasi-2D Organic Conductor

M. de Souza[1], A. Brühl[1], Ch. Strack[1], B. Wolf[1], D. Schweitzer[2], and M. Lang[1]
[1] *Physikalisches Institut, J.W. Goethe-Universität Frankfurt(M), FOR 412, D-60054 Frankfurt am Main, Germany and*
[2] *3. Physikalisches Institut, Universität Stuttgart, D-70550 Stuttgart, Germany*

(Dated: February 6, 2008)

Discontinuous changes of the lattice parameters at the Mott metal-insulator transition are detected by high-resolution dilatometry on deuterated crystals of the layered organic conductor $\kappa$-(BEDT-TTF)$_2$Cu[N(CN)$_2$]Br. The uniaxial expansivities uncover a striking and unexpected anisotropy, notably a zero-effect along the in-plane $c$-axis along which the electronic interactions are relatively strong. A huge thermal expansion anomaly is observed near the end-point of the first-order transition line enabling to explore the critical behavior with very high sensitivity. The analysis yields critical fluctuations with an exponent $\tilde{\alpha} \simeq 0.8 \pm 0.15$ at odds with the novel criticality recently proposed for these materials [Kagawa *et al.*, Nature **436**, 534 (2005)]. Our data suggest an intricate role of the lattice degrees of freedom in the Mott transition for the present materials.

PACS numbers: 72.15.Eb, 72.80.-r, 72.80.Le, 74.70.Kn

The Mott metal-insulator (MI) transition has been the subject of intensive research for many years, see e.g. [1] for a review. Materials intensively discussed in this context include transition metal oxides, notably Cr-doped $V_2O_3$, and, recently, organic $\kappa$-(BEDT-TTF)$_2$X charge-transfer salts [2, 3, 4, 5]. Here BEDT-TTF (or simply ET) denotes bis(ethylenedithio)tetrathiafulvalene and X a monovalent anion. For the latter substances, pressure studies revealed a first-order metal-insulator transition line $T_{MI}(P)$ [2, 3, 4, 5, 6], indicative of a bandwidth-controlled Mott transition [7, 8], and suggest a second-order critical endpoint $(P_0, T_0)$ [2, 3, 4, 5] with remarkable properties. Particularly striking was the observation of a pronounced softening of the $c_{22}$ elastic mode [4]. Although acoustic and lattice anomalies are expected [9, 10] at the Mott transition in *response* to the softening of the electronic degrees of freedom, the actual role of the lattice for the Mott transition in real materials remains illusive. In addition, an unconventional Mott criticality was proposed for the present organic salts [11] and attributed to their quasi-twodimensional (quasi-2D) electronic character.

In this Letter we report, for the first time, the direct observation of lattice anomalies at the Mott transition in a $\kappa$-(ET)$_2$X organic conductor and explore, via a sensitive thermodynamic probe, the criticality near $(P_0, T_0)$.

For the thermal expansion measurements, a high-resolution capacitive dilatometer (built after [12]) was used, enabling the detection of length changes $\Delta l \geq 10^{-2}$ Å. Owing to the experimental difficulties posed by accomplishing high-resolution dilatometric measurements under variable pressure, use was made of the possibility of applying chemical pressure. To this end, single crystals of $\kappa$-(d8-ET)$_2$Cu[N(CN)$_2$]Br were synthesized with deuterium atoms replacing the protons in the terminal ethylene groups. These fully deuterated salts, referred to as d8-Br in the following, are known to be situated very close to the MI transition [13]. First, deuterated (98%) ET molecules were prepared according to [14, 15] using multiple recrystallization for the intermediate steps. Next, single crystals were synthesized along an alternative preparation route described recently for the protonated variant h8-Br [16]. The grade of deuteration was checked by infrared reflection spectroscopy both on the deuterated ET material [17] as well as on the d8-Br single crystals [18], and found to be at least 98%. For the present study, crystals of two independently prepared batches were used: crystal #1 (batch A2907) and #3 (A2995). The crystals have the shape of flat distorted hexagons with dimensions of about $1 \times 1 \times 0.4$ mm$^3$. The pressure exerted on the crystal by the dilatometer ranges from 1 to 6 bar. A preliminary account on a second crystal from batch A2907 was given in [19]. The resistivity was studied by employing a standard four-terminal ac-technique. All measurements, unless stated otherwise, were carried out after cooling through the glass transition at $T_g \sim 77$ K with a very low rate of -3 K/h (thermal expansion) and -6 K/h (resistivity) to rule out cooling-rate dependent effects, see [20].

The interlayer resistivity $\rho_\perp$ for crystal #1 is shown in the lower part of Fig. 1. Upon cooling, $\rho_\perp$ passes over a maximum around 45 K, then rapidly drops and flattens around 30 K. The resistivity remains metallic down to about 20 K, below which the slope sharply increases (cf. upper inset in Fig. 1) indicating the transition into an insulating state. A similar $\rho_\perp$ was found for crystal #3 and the crystal studied in [19] including the vanishing of $\rho_\perp$ below about 11.5 K. A zero resistivity accompanied by a tiny signature in the $\alpha_i$ data is consistent with percolative superconductivity in a minor metallic phase coexisting with an antiferromagnetic/insulating ground state for d8-Br [21], cf. the phase diagram in Fig. 3.

The main features in the resistivity have their clear correspondence in the coefficient of thermal expansion, $\alpha = l^{-1} dl/dT$, also shown in Fig. 1 along the $a$-axis of crystal #1. The flattening of $\rho_\perp$ is accompanied by a

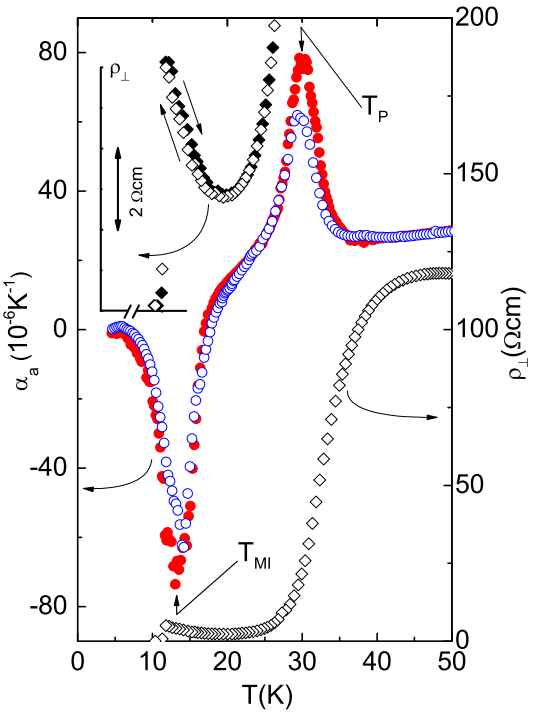


FIG. 1: (Color online) In-plane $a$-axis expansivity, $\alpha_a$ (full circles), (left scale) and interlayer resistivity, $\rho_\perp$, (right scale) for $\kappa$-(d8-ET)$_2$Cu[N(CN)$_2$]Br crystal #1 together with $\alpha_a$ data for crystal #3 (open circles). Upper inset: blow-up of low-$T$ $\rho_\perp(T)$ data on the same $T$ scale as used in the main panel.

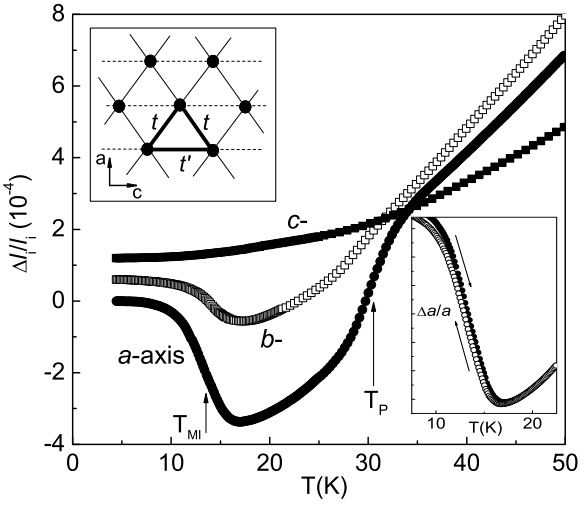


FIG. 2: Relative length changes for $\kappa$-(d8-ET)$_2$Cu[N(CN)$_2$]Br crystal #1 along the in-plane $a$- and $c$-, and out-of-plane $b$-axis. The data have been offset for clarity. Lower inset shows hysteretic behavior in $\Delta a/a$ at $T_{MI}$ measured at very low sweeping rates of $\pm 1.5$ K/h. Upper inset depicts the 2D triangular-lattice dimer model with transfer integrals $t$ and $t'$.

huge peak in $\alpha(T)$ centered at a temperature referred to as $T_p$ in the following around 30 K. As will be discussed below, this effect can be assigned to a second-order phase transition. Upon further cooling, $\alpha_a(T)$ reveals an even bigger negative peak indicating yet another phase transition. The accompanying change in $\rho_\perp$ from metallic to insulating behavior suggests this peak to be due to the MI transition. This is consistent with measurements under magnetic fields up to 10 T (not shown) leaving the peak position unaffected. A very similar $\alpha_a(T)$ behavior is observed for #3, although with slightly reduced ($\sim$ 20%) peak anomalies and minor shifts in $T_p$ and $T_{MI}$, cf. Fig. 1. More insight into the character of the transitions can be gained by looking at the relative length changes $\Delta l_i(T)/l_i = (l_i(T)$ - $l_i(300\,K))/l_i(300\,K)$, $(i = a, b, c)$ shown in Fig. 2 for crystal #1. The dominant effects occur along the in-plane $a$-axis, i.e. parallel to the anion chains. Here a pronounced s-shaped anomaly is revealed at $T_p$ which lacks any sign of hysteresis upon cooling and warming – generic features of a second-order phase transition with strong fluctuations. On further cooling through $T_{MI}$, the $a$-axis shows a rapid increase of about $\Delta a/a = 3.5 \cdot 10^{-4}$ within a narrow temperature range, indicative of a slightly broadened first-order transition. The observation of a small but significant hysteresis of about 0.4 K (cf. lower inset Fig. 2), which complies with the hysteresis in $\rho_\perp(T)$ (upper inset Fig. 1), confirms the first-order character. The corresponding anomalies along the $b$-axis are less strongly pronounced. Surprisingly, for the second in-plane $c$-axis, anomalous behavior in $\Delta l/l$ can be discerned neither at $T_p$ nor at $T_{MI}$. The same anisotropy was found for the second crystal of batch A2907 studied in [19] (not shown), on which all three uniaxial expansion coefficients had been determined.

Figure 2 reveals that the anomalies at $T_p$ and $T_{MI}$ are correlated in size, albeit with reversed sign, suggesting that they are intimately related to each other. In addition, the data disclose a striking in-plane anisotropy. Given the quasi-2D electronic structure as shown in the upper inset of Fig. 2, characterized by dimers on an anisotropic triangular lattice [8], the latter is a very remarkable and unexpected result: The dominant response in the $a$-axis, along which no direct dimer-dimer overlap exists, means that the diagonal electronic interactions along the $c \pm a$ directions, $t$, have to be involved in this process. Since these interactions have a strong component also along the $c$-axis, which is likely to be even softer than the anion-chain $a$-axis [22], a significant $c$-axis response would be expected at $T_{MI}$. A zero-effect along the $c$-axis is even more amazing as there is a relatively strong direct dimer-dimer interaction $t'$ along this axis, cf. upper inset of Fig. 2. Thus, to account for a zero $c$-axis response within a 2D electronic model would imply an accidental cancellation of counteracting effects associated with $t$ and $t'$, which seems very unlikely. Furthermore, it is not obvious how these in-plane interactions may cause

the comparatively strong effect in the interlayer $b$-axis, along which the lattice is expected to be even more stiff [22]. These observations suggest that a coupling of the $\pi$-electrons to other degrees of freedom has to be taken into account to understand the MI transition here.

Before discussing further implications of our observations, the MI-transition temperature $T_{MI}$ is determined. As Fig. 2 demonstrates, the transition is not very sharp but rather spans a range of several Kelvin – an effect which is very similar for both crystals studied here and the one explored in [19]. A broadening of signatures in $T$-dependent measurements, as opposed to isothermal pressure sweeps, would be naturally expected given the steepness of $T_{MI}(P)$, cf. Fig. 3. However, the width of about 5.6 K of the $\Delta l_a/l_a$ jump (10-90%), which transforms into a pressure interval of about 2 MPa employing a slope $dT_{MI}/dP = -2.7 \pm 0.1$ K/MPa around 14 K (cf. Fig. 3), is even smaller than the transition range seen in acoustic measurements as a function of pressure [4] (cf. hatched area in Fig. 3), but is comparable with a width of about 1.4 MPa as read off the resistivity data in [5]. These smearing effects have been attributed to a region of coexistence between insulating and metallic phases [3], as indeed observed via real-space imaging [24]. For lack of a well-founded procedure to treat the broadened transitions, the position of the $\alpha(T)$ minimum is chosen as the thermodynamic transition temperature. Employing literature results on $T_{MI}(P)$ [25], the so-derived values of $T_{MI} = (13.5 \pm 0.8)$ K, (#1) and $(14.1 \pm 0.8)$ K, (#3) can be used to pinpoint the position of the present d8-Br crystals on the pressure axis in Fig. 3. Within the uncertainties implied in this procedure, the crystals are located very close to the critical pressure $P_0$ as determined by the various pressure studies [2, 3, 4, 5]. The significance of this finding is twofold. First, it demonstrates that the anomaly at $T_p$ reflects the lattice response at $(P_0, T_0)$. Second, as this point is part of the $T_{MI}$ line, it provides a natural explanation for the intimate interrelation of the anomalies at $T_p$ and $T_{MI}$ inferred from Fig. 2.

The huge anomaly at $T_p \simeq T_0$, exceeding the background by a factor 3-4, enables us to explore the criticality at $(P_0, T_0)$ with extraordinarily high sensitivity. To this end, the phase transition anomaly in $\alpha_a(T)$, shown for the crystals #1 and #3 in Fig. 4 on expanded scales, is analyzed in terms of a power-law behavior in the variable $t = (T - T_0)/T_0$. This approach is based on the proportionality of $\alpha(T)$ to the specific heat, $C(T)$, implying that the same scaling laws apply at $T_0$, as verified by various groups, see, e.g. [26, 27].

The data sets in Fig. 4 reveal a steep increase in the slope of $\alpha(T)$ on the outer flanks of the maximum. Closer to the center of the peak, however, the slope is reduced giving rise to a rounded maximum. Such broadening effects are generally encountered in the immediate vicinity of the transition and attributed to sample inhomogeneities. The rounding over a considerable temperature

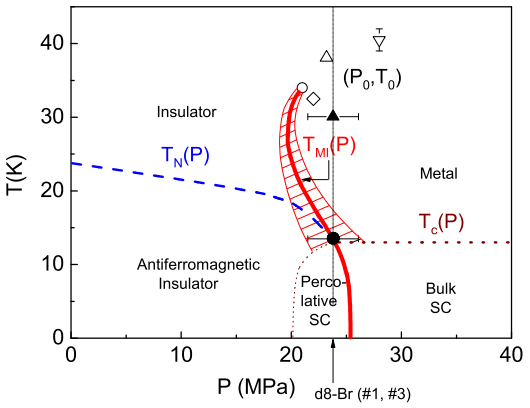


FIG. 3: (Color online) Phase diagram of $\kappa$-$(ET)_2X$ including the Néel transition at $T_N$ (dashed line) and the superconducting (SC) transition at $T_c$ (dotted line) from [2]. Thin solid lines, delimiting the hatched area, denote positions of acoustic anomalies [4]. The middle position (thick solid line) is used here as $T_{MI}(P)$ [25]. Closed symbols refer to anomalies at $T_{MI}$ and $T_p \simeq T_0$ of the d8-Br crystals #1 and #3 (same positions on the scale of the figure), while open symbols denote literature results for $(P_0, T_0)$: ($\diamond$) [2], ($\triangledown$) [3], ($\bigcirc$) [4], ($\triangle$) [5]. Vertical line indicates the $T$-sweeps performed here.

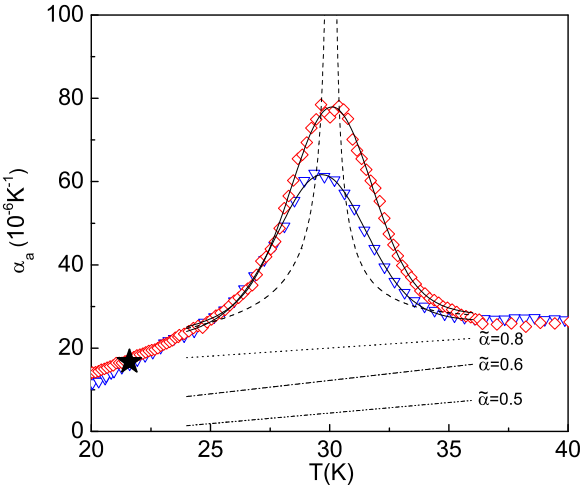


FIG. 4: (Color online) Expansivity along the $a$-axis for d8-Br crystals #1 ($\diamond$) and #3 ($\triangledown$) near $T_0$. Solid (dashed) lines are fits as described in the text for $\tilde{\alpha} = 0.8$ with (without for #1) a Gaussian distribution of $T_0$. Straight lines show background contributions implied in fits for $\tilde{\alpha}$ values given in the figure. Star marks universal background point discussed in the text.

range here demands particular attention. For the description of the data in the range 24 - 36 K, the function $\alpha = \frac{A^{\pm}}{\tilde{\alpha}}|t|^{-\tilde{\alpha}} + B + E \cdot T$ was used. This function contains the singular contribution with the amplitudes $A^+$ and $A^-$ for $t > 0$ and $t < 0$, respectively, and a linear term. The latter comes primarily from the phonons but can also include a small non-singular electronic contri-

bution. The smearing of the transition is accounted for by a Gaussian distribution for $T_0$, $G(\bar{T_0}, T_0, \delta T_0)$, centered at $\bar{T_0}$ with a width $\pm\delta T_0$. Applying the function $\int[\frac{A^{\pm}}{\tilde{\alpha}}|(T-T_0)/T_0|^{-\tilde{\alpha}}+B+E\cdot T]\cdot G(\bar{T_0}, T_0, \delta T_0)\cdot dT_0$, the data sets of crystal #1 and #3 were fitted simultaneously using the same exponent $\tilde{\alpha}$, the same ratio $A^+/A^-$, and an identical background for both crystals. A constraint for the background contribution can be derived by comparing the data in Fig. 4, with those of the d8-Br in [19] and h8-Br in [20]. All data sets intersect at a single point $T \simeq 21\,\mathrm{K}$, $\alpha \simeq 16 \cdot 10^{-6}\mathrm{K}^{-1}$, irrespective of the presence and size of the critical contribution at $T_0$, indicating that this point reflects the pure background. Thus a meaningful background should extrapolate to this universal point. A good fit to both data sets, also satisfying this background constraint, is obtained for $\tilde{\alpha} = 0.8$, $A^+/A^- = 0.79$, and $\bar{T_0} = 30.1\,\mathrm{K}$, $\delta T_0 = 1.59\,\mathrm{K}$ for #1 and $\bar{T_0} = 29.6\,\mathrm{K}$, $\delta T_0 = 1.74\,\mathrm{K}$ for #3, cf. Fig. 4. We stress that $\tilde{\alpha}$ values in the range 0.65 - 0.95, with small changes in the other parameters accordingly, result in fits of similar quality and still comply with the background constraint. In contrast, the residual of the fit increases substantially upon decreasing $\tilde{\alpha}$ to well below 0.65. This is accompanied by a suppression of the background to even negative values for $\tilde{\alpha} < 0.5$, clearly incompatible with the background constraint, see, e.g., the background implied in the fits for $\tilde{\alpha} = 0.6$ and 0.5 in Fig. 4. As clearly indicated by these simultaneous fits, and confirmed by independent fits to the individual data sets for crystals #1 and #3, a large positive $\tilde{\alpha}$ value is the only possible, physically meaningful description of the expansivity data.

The critical exponent derived here of $\tilde{\alpha} \simeq 0.8 \pm 0.15$ is much larger than those of known universality classes with $-0.12 \leq \tilde{\alpha} \leq 0.14$ and the mean-field value $\tilde{\alpha} = 0$ observed at the Mott critical endpoint of Cr-doped $V_2O_3$ [28]. In particular, it greatly conflicts with the criticality reported in [11] for pressurized X = Cu[N(CN)$_2$]Cl. Employing the exponent identity $\tilde{\alpha}+2\beta+\gamma = 2$ [29] the exponents found there of $(\delta, \beta, \gamma) \approx (2, 1, 1)$ give $\tilde{\alpha} = -1$. The reason for this discrepancy is unclear but might be related to the significant broadening effects [30], which have not been included in the analysis in [11]. The exponent found here, however, is rather close to $\tilde{\alpha} = 0.5$ expected for a tricritical point [31]. Such a scenario would imply a symmetry breaking associated with $T_{MI}$ for which no evidence has yet been supplied. Interestingly, an even larger exponent $\tilde{\alpha} = 0.93$ was reported for $La_{0.7}Ca_{0.3}MnO_3$ [27], also characterized by a strong electron-phonon coupling, showing a similar $\alpha(T)$ anomaly as the one observed here.

In summary, high-resolution dilatometry on deuterated $\kappa$-(ET)$_2$Cu[N(CN)$_2$]Br crystals reveals discontinuous changes of the lattice parameters at the Mott transition. The data disclose a striking anisotropy unlikely to be captured by a 2D purely electronic model. An analysis of the huge thermal expansion anomaly at the end-point of the first-order $T_{MI}$ line yields a critical exponent $\tilde{\alpha} \simeq 0.8 \pm 0.15$, markedly different from the criticality derived from transport measurements [11]. The unusually large $\tilde{\alpha}$ value together with the anomalous anisotropy of the lattice effects at $T_{MI}$ suggest an intricate role of the lattice in the Mott transition for the present materials.

M. de Souza acknowledges financial support from the Brazilian Research Foundation CAPES and the DAAD.


[1] M. Imada *et al.*, Rev. Mod. Phys. **70**, 1039 (1998).
[2] S. Lefebvre *et al.*, Phys. Rev. Lett. **85**, 5420 (2000).
[3] P. Limelette *et al.*, Phys. Rev. Lett. **91**, 016401 (2003).
[4] D. Fournier *et al.*, Phys. Rev. Lett. **90**, 127002 (2003).
[5] F. Kagawa, *et al.*, Phys. Rev. B **69**, 064511 (2004).
[6] H. Ito *et al.*, J. Phys. Soc. Jpn. **9**, 2987 (1996).
[7] K. Kanoda, Hyperfine Interact. **104**, 235 (1997).
[8] H. Kino *et al.*, J. Phys. Soc. Jpn. **64**, 2726 (1995).
[9] S.R. Hassan *et al.*, Phys. Rev. Lett. **94**, 036402 (2005).
[10] J. Merino *et al.*, Phys. Rev. B **62**, 16442 (2000).
[11] F. Kagawa *et al.*, Nature **436**, 534 (2005).
[12] R. Pott *et al.*, J. Phys. E **16**, 444 (1983).
[13] A. Kawamoto *et al.*, Phys. Rev. B **55**, 14140 (1997).
[14] K. Hartke *et al.*, Chem. Ber. **113**, 1898 (1980).
[15] M. Mizuno *et al.*, J. Chem. Sci. Commun. **1978**, 18 (1978).
[16] Ch. Strack *et al.*, Phys. Rev. B **72**, 054511 (2005).
[17] S. Gärtner *et al.*, Synth. Met. **44**, 227 (1991).
[18] E. Grießhaber, Dissertation, University Stuttgart (2000), unpublished.
[19] M. Lang *et al.*, *Proceedings of the 8th Intern. Conf. on Materials and Mechanisms of Superconductivity - High Temperature Superconductors*, Physica C, in press.
[20] J. Müller *et al.*, Phys. Rev. B **65**, 144521 (2002).
[21] K. Miyagawa *et al.*, Phys. Rev. Lett. **89**, 017003 (2002).
[22] For the related X = Cu(NCS)$_2$ salt, the uniaxial compressibilities $k_i$ are strongly anisotropic [23] with $k_1 : k_2 : k_3 = 1 : 0.53 : 0.17$, and $i = 1$ and 2 the in-plane axis perpendicular and parallel to the anion chains, respectively, and $i = 3$ along the long axis of the ET molecules.
[23] D. Chasseau *et al.*, Synth. Met. **41 − 43**, 2039 (1991).
[24] T. Sasaki *et al.*, Phys. Rev. Lett. **92**, 227001 (2005).
[25] Due to the finite range of phase coexistence around $T_{MI}$, the comparison of the thermodynamically determined $T_{MI}$ values here with those derived from transport experiment [2, 3] may cause some ambiguity. We therefore refer to $T_{MI}(P)$ as the mean value (thick solid line in Fig. 3) of acoustic anomalies [4].
[26] V. Pasler *et al.*, Phys. Rev. Lett. **81**, 1094 (1998).
[27] J.A. Souza *et al.*, Phys. Rev. Lett. **94**, 207209 (2005).
[28] P. Limelette *et al.*, Science **302**, 89 (2003).
[29] L.P. Kadanoff *et al.*, Rev. Mod. Phys. **39**, 395 (1967).
[30] In view of the huge $\partial T_0/\partial P$ of approximately 2-3K/MPa, cf. Fig. 3, weak strain fields due to minor sample inhomogeneities can give rise to a broad distribution of $T_0$ values as observed here.
[31] K. Huang, *Statistical Mechanics* (Wiley, New York, 1987) $2^{nd}$ ed., Chap. 17.6.